Three-Dimensional Coherent X-Ray Diffraction Imaging of Molten Iron in Mantle Olivine at Nanoscale Resolution

Huaidong Jiang,[1] Rui Xu,[2] Chien-Chun Chen,[2] Wenge Yang,[3] Jiadong Fan,[1] Xutang Tao,[1] Changyong Song,[4] Yoshiki Kohmura,[4] Tiqiao Xiao,[5] Yong Wang,[5] Yingwei Fei,[6] Tetsuya Ishikawa,[4] Wendy L. Mao,[7,8] and Jianwei Miao[2,*]

[1]*State Key Laboratory of Crystal Materials, Shandong University, Jinan 250100, China*
[2]*Department of Physics and Astronomy and California NanoSystems Institute, University of California, Los Angeles, California 90095, USA*
[3]*HPSynC, Geophysical Laboratory, Carnegie Institution of Washington, Argonne, Illinois 60439, USA*
[4]*RIKEN SPring-8 Center, 1-1-1, Kouto, Sayo, Hyogo 679-5148, Japan*
[5]*Shanghai Institute of Applied Physics, Chinese Academy of Sciences, Shanghai 201800, China*
[6]*Geophysical Laboratory, Carnegie Institution of Washington, Washington, DC 20015, USA*
[7]*Department of Geological and Environmental Sciences, Stanford University, Stanford, California 94305, USA*
[8]*Photon Science and Stanford Institute for Materials and Energy Sciences, SLAC National Accelerator Laboratory, Menlo Park, California 94025, USA*

(Received 6 December 2012; published 13 May 2013)

We report quantitative 3D coherent x-ray diffraction imaging of a molten Fe-rich alloy and crystalline olivine sample, synthesized at 6 GPa and 1800 °C, with nanoscale resolution. The 3D mass density map is determined and the 3D distribution of the Fe-rich and Fe-S phases in the olivine-Fe-S sample is observed. Our results indicate that the Fe-rich melt exhibits varied 3D shapes and sizes in the olivine matrix. This work has potential for not only improving our understanding of the complex interactions between Fe-rich core-forming melts and mantle silicate phases but also paves the way for quantitative 3D imaging of materials at nanoscale resolution under extreme pressures and temperatures.

DOI: 10.1103/PhysRevLett.110.205501 PACS numbers: 61.05.C−, 07.35.+k, 61.46.−w, 68.37.Yz

Investigation of the structure, composition, density, and evolution of Earth and planetary interiors can be a challenging task due to the difficulties in accessing the extreme conditions that exist in these regions. To gain a better understanding of planetary core evolution and the potential of percolation as a significant core-forming mechanism, a number of experiments have been conducted to explore the structure and behavior of molten Fe-rich alloy trapped between silicate grains [1–8]. However, the formation mechanism of terrestrial cores is still not fully understood. For example, previous studies suggest that melt resides in channels along silicate grain edges based on 2D images of melt distribution [9,10], but observations of olivine plus metallic melt aggregates indicate that melt is present both in grain edge channels and as grain boundary films [2,11]. To probe the 3D structural information, synchrotron-based x-ray tomography has been used to image the melt distribution [12–14]. However, the spatial resolution of this imaging technique was limited to be ~ 0.7 μm.

To determine the 3D structure of the melt distribution in mantle rocks at higher spatial resolution and with better image contrast, coherent diffraction imaging (CDI), also known as coherent diffraction microscopy, is an ideal method. CDI is a lensless imaging technique in which the diffraction pattern of a noncrystalline specimen or a nanocrystal is first measured and then directly phased to obtain an image [15–19]. The well-known phase problem is solved by combining the oversampling method with iterative algorithms [20]. In this Letter, we apply CDI to 3D structural studies of an olivine-Fe-S sample synthesized at 6 GPa and 1800 °C, and observe the 3D distribution of Fe-rich and Fe-S phases in the olivine matrix with nanoscale resolution.

To mimic the conditions of Earth's upper mantle, the sample used in this study was synthesized from 80 wt% San Carlos olivine [$(Mg_{0.88}Fe_{0.12})_2SiO_4$] mixed with 20 wt%Fe + 10 wt%S in a multianvil apparatus at 6 GPa and 1800 °C for 1 h (see the Supplemental Material [21]). Since Fe-S has a lower melting temperature than San Carlos olivine, it will melt during the high pressure and temperature treatment while the silicate remains solid [22–24]. The sample was then crushed into small pieces and supported on 30 nm thick Si_3N_4 membranes. Well-isolated samples were chosen for the CDI experiment, which was conducted on an undulator beam line at the SPring-8 with E = 5 keV. Figure 1(a) shows a representative 2D x-ray diffraction pattern of an olivine-Fe-S sample. A high resolution image with a pixel size of 16.3 nm [Fig. 1(b)] was directly reconstructed by using an oversampling based iterative algorithm [25] and represents a 2D projection of a 3D sample. To confirm the CDI reconstruction, a scanning transmission x-ray microscope (STXM) experiment was performed on the same sample at the Shanghai Synchrotron Radiation Facility (SSRF) [26]. By scanning the sample relative to a focused x-ray beam at 707 eV, the STXM image was acquired with a

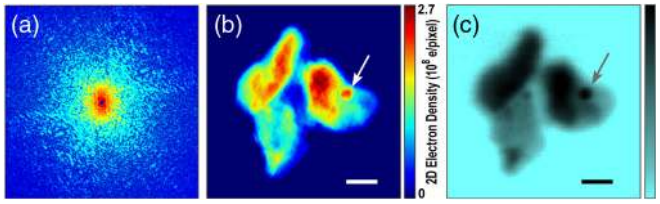

FIG. 1 (color online). (a) A representative coherent x-ray diffraction pattern measured from an olivine-Fe-S sample. (b) A 2D projection of the olivine-Fe-S sample reconstructed from (a), showing different electron density. (c) STXM image of the same sample. Scale bar is 500 nm.

pixel size of ~30 nm, shown in Fig 1(c). The overall morphology (size and shape) and the density contrast of the olivine-Fe-S sample in STXM image [Fig. 1(c)] are in good agreement with the CDI image [Fig. 1(b)]. There are some slight differences between these two images because the spatial resolution, image contrast mechanism, and the probing x-ray energy are different between the two imaging techniques.

To obtain the 3D structural information of the olivine-Fe-S sample, we acquired a tilt series of 27 x-ray diffraction patterns from the sample with a tilt range of $-69.4°$ to $+69.4°$. Each individual x-ray diffraction pattern in the tilt series was phased to obtain a high resolution 2D image [25]. Note that a more accurate iterative algorithm, termed oversampling smoothness (OSS), has recently been developed to phase diffraction patterns [27]. The series of the 2D images was aligned to the tilt axis with the center of mass technique [28–30], and was then reconstructed to obtain a 3D image by the equally sloped tomography (EST) method [29–32]. EST is a Fourier-based iterative algorithm, allowing good quality tomographic reconstructions from a limited number of projections with a missing wedge. To examine the 3D reconstruction quality, we projected it back to obtain 2D images, which are consistent to the original images. Figure 2 and movie S1 in the Supplemental Material [21] show isosurface renderings of the 3D reconstructed image of the olivine-Fe-S sample. The 3D resolution of the reconstruction was quantified to be ~32.5 nm (2 pixels) in the X and Y axes and ~48.8 nm (3 pixels) in the Z axis (Fig. 3). The volume of the sample was determined to be $\sim 2.44 \times 2.31 \times 0.78\ \mu m^3$. This sample consists of three micron-sized particles with irregular shapes and rough surfaces, two of which are loosely connected (Fig. 2 and movie S1 in the Supplemental Material [21]. The 3D shape, surface morphology, and volume of the particles are related to the high pressure and temperature treatment process.

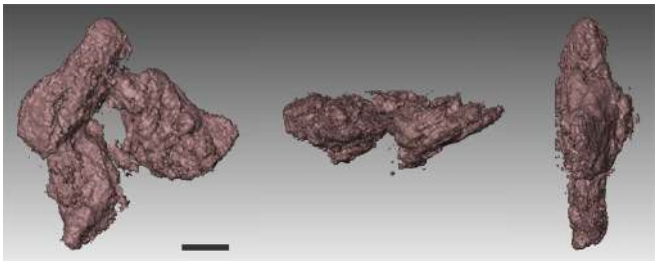

FIG. 2 (color online). Iso-surface renderings of the 3D reconstructed image, showing the front, top, and side views of the olivine-Fe-S sample. The sample consists of three micron-sized particles exhibiting irregular shapes and rough surfaces, two of which are loosely connected. Scale bar is 500 nm.

Experimental characterization of the density of Earth materials under geologically relevant pressure and temperature conditions is crucial for successful interpretation of the seismic models. We thus performed a quantitative analysis of 3D density distribution in the olivine-Fe-S sample. By measuring the incident x-ray flux and quantifying the diffraction intensities, we were able to directly determine the 3D electron density of the olivine-Fe-S sample [19,33] (also, see the Supplemental Material [21]). Based on the unit-cell volumes of individual phases and chemical composition of the materials, the average mass density of the olivine-Fe-S sample was determined to be ~3.58 g/cm^3 (see the Supplemental Material [21]), which is in good agreement with that reported elsewhere [34]. Figure 4(a) shows the 3D mass density distribution in several slices of the olivine-Fe-S sample.

To confirm the Fe distribution inside the olivine matrix, we performed element specific imaging of the same sample using a dual-energy STXM with x-ray energy of 703.75 eV and 709 eV [26], which are below and above the Fe L_3 edge. Figure 4(b) shows the 2D Fe distribution in the

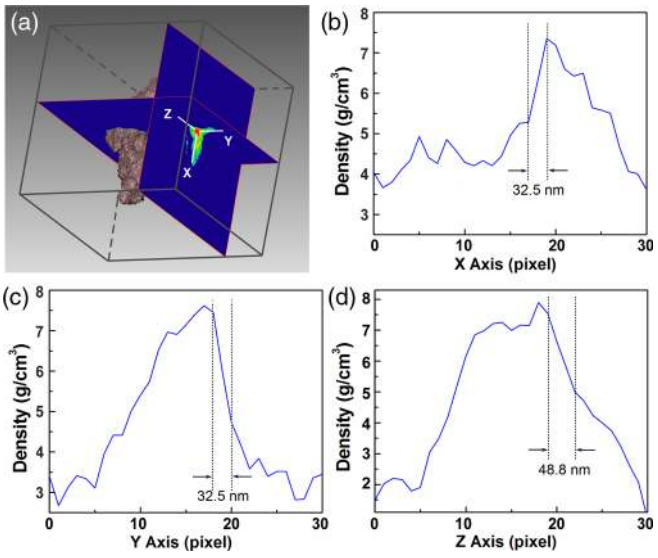

FIG. 3 (color online). Quantification of the 3D resolution. (a) The density variation across a Fe-rich phase region is plotted along the X, Y, and Z axes to estimate the 3D resolution of the reconstructed olivine-Fe-S sample. (b), (c) Resolution of ~32.5 nm (i.e., 2 pixels) is achieved along the X and Y axes. (d) A resolution of ~48.8 nm (i.e., 3 pixels) is achieved along the Z axis.

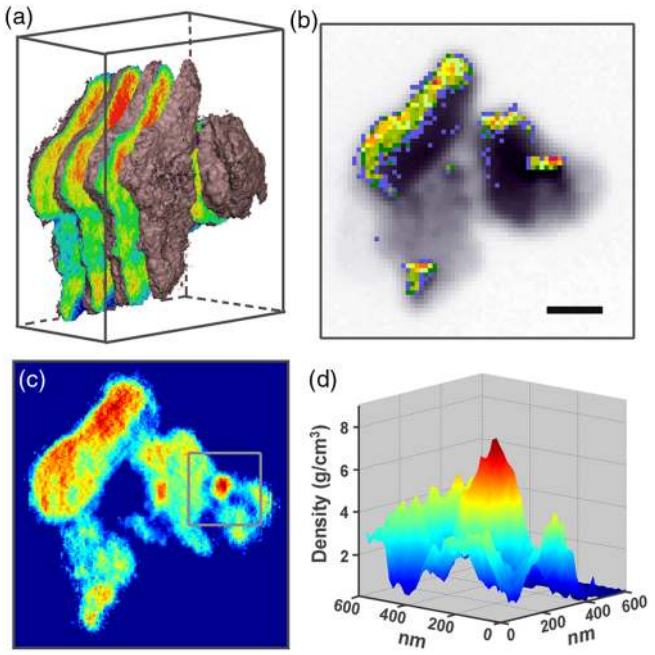

FIG. 4 (color online). 3D internal structure of the olivine-Fe-S sample. (a) 3D mass density distribution in several slices of the olivine-Fe-S sample (the red, yellow, and blue colors in the online figure represent the high, medium, and low mass densities, respectively). (b) 2D dual-energy STXM image of the sample acquired near the Fe L_3 edge: 703.75 eV and 709 eV. The colored areas indicate the existence of the Fe-rich phase within the sample. Scale bar is 500 nm. (c) A 16.3 nm thick slice showing the distribution of the mass density in the olivine-Fe-S sample. (d) Zoom-in view of the square region (600×600 nm^2) in (c), showing the variation of mass density and the existence of Fe-rich and Fe-S phases.

sample where Fe is mainly distributed at the edges of the particles. The dual-energy STXM image is consistent with the 16.3 nm thick slice of the CDI reconstruction [Fig. 4(c)]. The slight differences between the two images [Figs. 4(b) and 4(c)] are mainly due to (i) being taken at different x-ray energies, (ii) the fact that the dual-energy STXM image represents a 2D projection of the 3D Fe distribution that does not contain the depth information of the sample, while Fig. 4(c) shows the Fe distribution in a 16.3 nm thick slice of the 3D sample, and (iii) the CDI image has a higher resolution than the STXM one. Figure 4(d) shows the mass density distribution of the square region in Fig. 4(c), in which the high mass density is concentrated near the center of an islandlike region. The islandlike region represents a Fe and Fe-S enriched melt pocket which, according to previous theoretical and experimental studies [13,35], is surrounded by three or more grains. The melt pocket size of the 3D Fe-rich phase was estimated to be $244 \times 277 \times 310$ nm^3.

To reveal the 3D melt composition and distribution in the olivine and molten Fe-S sample, the 3D mass density map was quantitatively analyzed. Figure 5(a) and movie S2 in the Supplemental Material [21]) show 3D volume renderings of the olivine-Fe-S sample, exhibiting the Fe-rich phase, Fe-S phase, and olivine distribution. Figure 5(b) and movie S3 [21] show a zoomed view of the 3D volume renderings in a $600 \times 600 \times 600$ nm^3 volume [corresponding to the square region in Fig. 4(c)]. The histogram of the Fe-rich phase, Fe-S phase, and olivine distribution in Fig. 5(b) was also obtained, shown in Fig. 5(c). Previous studies suggested that molten Fe tends to form small isolated spheres at relatively low pressure, which could not percolate through solid silicate matrix and form a connective network [4]. In our high-resolution 3D structural studies, the molten Fe not only forms isolated spheres, but also exhibits other irregular 3D shapes and sizes in the olivine matrix at the nanoscale resolution. The zoomed view [Fig. 4(d)] and quantitative analysis also suggest that the density distribution of Fe-rich and Fe-S phases changes continuously instead of abruptly. The formation of these molten Fe is related to the local temperature, pressure, and geometry within the olivine matrix as well as the 3D microscopic percolation mechanism at the nanoscale level.

In summary, we performed CDI and STXM measurements of molten Fe-rich alloy and mantle olivine to investigate the 3D melt distribution at the nanoscale resolution. CDI provides 3D local structure at high resolution, while STXM offers the element-specific imaging capability. The combined results provide direct evidence of the existence of 3D Fe-rich and Fe-S phases in the olivine-Fe-S sample

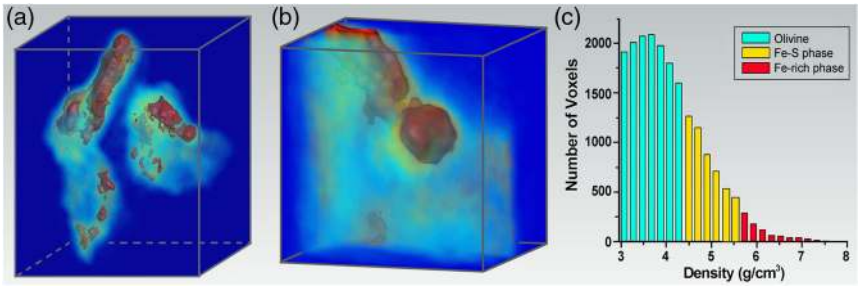

FIG. 5 (color online). (a) 3D volume rendering of the olivine-Fe-S sample, showing the Fe-rich phase, Fe-S phase, and olivine distribution. (b) A zoomed view of a $600 \times 600 \times 600$ nm^3 volume inside the olivine-Fe-S sample [corresponding to the square region in Fig. 4(c)]. (c) A histogram of the Fe-rich phase, Fe-S phase and olivine distribution in (b).

at the nanoscale resolution. Furthermore, we observed that the 3D morphology of the Fe-rich phase exhibits varied 3D shapes and size in the olivine matrix. While the spatial resolution reported here is ~32.5 nm in the X and Y axes and ~48.8 nm in the Z axis, the ultimate resolution of CDI is only limited by how far the sample can diffract [15–20]. By using more advanced coherent x-ray sources, significantly higher resolution can in principle be achieved. Although transmission electron microscopy has been used to image olivine grain boundaries and olivine-basalt aggregates at much higher resolution [36,37], it only provides 2D projection information. Through a combination of scanning transmission electron microscopy and EST, electron tomography has recently achieved 3D imaging of nanoscale materials at atomic resolution [29,30], but the sample has to be thin enough to avoid dynamical scattering effects. On the other hand, synchrotron-based x-ray tomography has been applied to image 3D melt distribution in thick partially molten rocks with a reduced resolution of ~0.7 μm [12–14]. Therefore, there is an important gap between electron microscopy and synchrotron x-ray tomography to investigate the structural information of Earth's mantle in terms of sample thickness and spatial resolution. Due to the large penetration depth of x rays and its high spatial resolution and image contrast ability, CDI is an ideal technique to bridge this gap [15–20]. With further development, we expect CDI to expand our comprehensive understanding of the critical structural and morphological features of Earth's materials under higher pressures and temperatures.

We thank H. K. Mao for many stimulating discussions and the staff at Shanghai Synchrotron Radiation Facility beam line 8U for their assistance with data acquisition. This work was partially supported by the DOE, BES, RIKEN in Japan, the National Natural Science Foundation of China (No. 51002089), the Natural Science Funds for Distinguished Young Scholar of Shandong Province (JQ201117), and the Program for New Century Excellent Talents (NCET-11-0304). W. L. M. is supported by NSF-EAR-1055454. W. Y. is supported by EFree, an Energy Frontier Research Center funded by the U.S. DOE-BES under Grant No. DE-SC0001057. Use of the RIKEN beam line (BL29XUL) at SPring-8 was supported by RIKEN.

*miao@physics.ucla.edu

[1] B. Minarik, Nature (London) **422**, 126 (2003).
[2] D. Bruhn, N. Groebner, and D. L. Kohlstedt, Nature (London) **403**, 883 (2000).
[3] C. Holzapfel, D. C. Rubie, D. J. Frost, and F. Langenhorst, Science **309**, 1707 (2005).
[4] W. G. Minarik, F. J. Ryerson, and E. B. Watson, Science **272**, 530 (1996).
[5] S. Karato and V. R. Murthy, Phys. Earth Planet. Inter. **100**, 61 (1997).
[6] R. Brett, Geochim. Cosmochim. Acta **48**, 1183 (1984).
[7] T. Yoshino, M. J. Walter, and T. Katsura, Nature (London) **422**, 154 (2003).
[8] R. J. M. Farla, I. Jackson, J. D. Fitz Gerald, U. H. Faul, and M. E. Zimmerman, Science **336**, 332 (2012).
[9] C. S. Smith, Metall. Rev. **9**, 1 (1964).
[10] N. von Bargen and H. S. Waff, J. Geophys. Res. **91**, 9261 (1986).
[11] M. R. Drury and J. D. Frtz Gerald, Geophys. Res. Lett. **23**, 701 (1996).
[12] J. J. Roberts, J. H. Kinney, J. Siebert, and F. J. Ryerson, Geophys. Res. Lett. **34**, L14306 (2007).
[13] W. Zhu, G. A. Gaetani, F. Fusseis, L. G. J. Montesi, and F. De Carlo, Science **332**, 88 (2011).
[14] H. C. Watson and J. J. Roberts, Phys. Earth Planet. Inter. **186**, 172 (2011).
[15] J. Miao, P. Charalambous, J. Kirz, and D. Sayre, Nature (London) **400**, 342 (1999).
[16] J. Miao, T. Ishikawa, B. Johnson, E. Anderson, B. Lai, and K. Hodgson, Phys. Rev. Lett. **89**, 088303 (2002).
[17] I. K. Robinson and R. Harder, Nat. Mater. **8**, 291 (2009).
[18] H. N. Chapman and K. A. Nugent, Nat. Photonics **4**, 833 (2010).
[19] H. D. Jiang *et al.*, Proc. Natl. Acad. Sci. U.S.A. **107**, 11234 (2010).
[20] J. Miao, R. L. Sandberg, and C. Song, IEEE J. Sel. Top. Quantum Electron. **18**, 399 (2012).
[21] See Supplemental Material at http://link.aps.org/supplemental/10.1103/PhysRevLett.110.205501 for details.
[22] Y. Fei, C. M. Bertka, and L. Finger, Science **275**, 1621 (1997).
[23] T. M. Usselman, Am. J. Sci. **275**, 278 (1975).
[24] C. B. Agee, Phys. Earth Planet. Inter. **100**, 41 (1997).
[25] C. C. Chen, J. Miao, C. W. Wang, and T. K. Lee, Phys. Rev. B **76**, 064113 (2007).
[26] C. Xue *et al.*, Rev. Sci. Instrum. **81**, 103502 (2010).
[27] J. A. Rodriguez, R. Xu, C. C. Chen, Y. Zou, and J. Miao, J. Appl. Crystallogr. **46**, 312 (2013).
[28] C. C. Chen, J. Miao, and T. K. Lee, Phys. Rev. B **79**, 052102 (2009).
[29] M. C. Scott, C. C. Chen, M. Mecklenburg, C. Zhu, R. Xu, P. Ercius, U. Dahmen, B. C. Regan, and J. Miao, Nature (London) **483**, 444 (2012).
[30] C. C. Chen, C. Zhu, E. R. White, C. Y. Chiu, M. C. Scott, B. C. Regan, L. D. Marks, Y. Huang, and J. Miao, Nature (London) **496**, 74 (2013).
[31] J. Miao, F. Förster, and O. Levi, Phys. Rev. B **72**, 052103 (2005).
[32] Y. Zhao *et al.*, Proc. Natl. Acad. Sci. U.S.A. **109**, 18290 (2012).
[33] J. Miao, J. Amonette, Y. Nishino, T. Ishikawa, and K. O. Hodgson, Phys. Rev. B **68**, 012201 (2003).
[34] C. S. Zha, T. S. Duffy, R. T. Downs, H.-k. Mao, and R. J. Hemley, Earth Planet. Sci. Lett. **159**, 25 (1998).
[35] U. H. Faul and D. Scott, Mineral. Petrol. **151**, 101 (2006).
[36] M. CmíralJ. D. Fitz Gerald, U. H. Faul, and D. H. Green, Contrib. Mineral. Petrol. **130**,336 (1998).
[37] R. Wirth, Contrib. Mineral. Petrol. **124**, 44 (1996).